Journal of Hazardous Materials 189 (2011) 755–763

Contents lists available at ScienceDirect

Journal of Hazardous Materials

journal homepage: www.elsevier.com/locate/jhazmat

Arsenate removal from aqueous solution by cellulose-carbonated hydroxyapatite nanocomposites

Mahamudur Islam [a,*], Prakash Chandra Mishra [a], Rajkishore Patel [b]

[a] Department of Chemistry, Purushottam Institute of Engineering & Technology, Purushottam Vihar, 10th km, Highway – 10, Mandiakudar, Kansbahal, Rourkela 770034, Orissa, India
[b] Department of Chemistry, National Institute of Technology, Rourkela 769008, Orissa, India

ARTICLE INFO

Article history:
Received 7 November 2010
Received in revised form 11 March 2011
Accepted 14 March 2011
Available online 22 March 2011

Keywords:
Adsorption
Arsenate
Hydroxyapatite
Kinetic study
Thermodynamic parameters

ABSTRACT

Microwave-assisted synthesis of the cellulose-carbonated hydroxyapatite nanocomposites (CCHA) with CHA nanostructures dispersed in the cellulose matrix was carried out by using cellulose solution, $CaCl_2$, and NaH_2PO_4. The cellulose solution was previously prepared by the dissolution of microcrystalline cellulose in NaOH–urea aqueous solution. Study was carried out to evaluate the feasibility of synthetic CCHA for As(V) removal from aqueous solution. Batch experiments were performed to investigate effects of various experimental parameters such as contact time (5 min – 8 h), initial As(V) concentration (1–50 mg/L), temperature (25, 35 and 45 °C), pH (2–10) and the presence of competing anions on As(V) adsorption on the synthetic CCHA. Kinetic data reveal that the uptake rate of As(V) was rapid at the beginning and equilibrium was achieved within 1 h. The adsorption process was well described by pseudo-first-order kinetics model. The adsorption data better fitted Langmuir isotherm. The maximum adsorption capacity calculated from Langmuir isotherm model was up to 12.72 mg/g. Thermodynamic study indicates an endothermic nature of adsorption and a spontaneous and favorable process. The optimum pH for As(V) removal was broad, ranging from 4 to 8. The As(V) adsorption was impeded by the presence of SiO_3^{2-}, followed by PO_4^{3-} and NO_3^-. The adsorption process appeared to be controlled by the chemical process.

1. Introduction

Arsenic contamination in natural water possesses a great threat to millions of people in many regions of the world [1,2]. Ground water contamination by arsenic has been a major problem in the northeastern parts of India like West Bengal, Assam and in few pockets of Orissa [3]. Arsenic occurs naturally in soils and water, and it also enters the environment due to anthropogenic activities. Common chemical forms of arsenic in the environment include arsenate (As(V)), arsenite (As(III)), dimethylarsinic acid (DMA), and monomethylarsenic acid (MMA). Epidemiological studies demonstrated that there is close link between the chronic exposure to arsenic in drinking water and some medical disorders and cancers [4,5]. Chronic arsenic poisoning can cause a lot of human health problems through either contaminated drinking water or agriculture products irrigated by contaminated water. Studies have demonstrated that chronic exposure to arsenic can lead to liver, lung, kidney, bladder, and skin cancers [6], cause cardio vascular system problems [7], and affect the mental development of children [8]. Accordingly, the U.S. Environmental Protection Agency revised the maximum contaminant level (MCL) for arsenic in drinking water from 10 to 50 μg/L in 2001 and required compliance with this level since January 2006 [9]. Recently, the state of New Jersey proposed that the MCL of arsenic in drinking water should be 5 μg/L to ensure the health of people [10].

Arsenic removal from water is an important subject worldwide, which has recently attracted great attentions. A variety of treatment processes has been developed for arsenic elimination from water, including coagulation (precipitation) [11], adsorption [12–14], ion exchange [15], membrane filtration [16], electrocoagulation [17,18], biological process [19], iron oxide-coated sand [20], high gradient magnetic separation [21] and natural iron ores [22], manganese greensand [23], etc. Coagulation and adsorption processes are most promising for arsenic removal from high-arsenic water because of the low cost and high efficiency, and are widely used in the developing countries. But, they have not been shown to deeply eliminate arsenic from water and to produce cleaned water with a very low arsenic concentration, say 10 μg/L. However, membrane filtration process could lower arsenic concentration in water from 48 to 1–2 μg/L [24], and ion exchange process could remove arsenic to levels lower than 5 μg/L for water with initial arsenic concentration of 87 μg/L [12], which are currently used in the developed countries. The other processes are still at a laboratory or pilot scale.

Owing to small size and high specific surface area, cellulose-carbonated hydroxyapatite nanocomposites [25] can effectively

* Corresponding author. Tel.: +91 8895270088; fax: +91 6624280625.
E-mail address: mahamudur.islam@gmail.com (M. Islam).

0304-3894/$ – see front matter © 2011 Elsevier B.V. All rights reserved.
doi:10.1016/j.jhazmat.2011.03.051

interact with arsenate ion, resulting in enhanced removal of arsenate from water. Hydroxyapatite, the most stable calcium phosphate compound at normal temperatures and the pH between 4 and 12, has the chemical formula, $Ca_{10}(PO_4)_6(OH)_2$, with the Ca/P ratio being 1.67. It is a compound of great interest mostly because of its chemical similarity to the mineral component of bones and hard tissues in mammals [26]. Nakahira et al. reported the removal of arsenic in geothermal water by using hydroxyapatite-based materials including the industrial waste, such as bovine bone and hydroxyapatite modified by a solid solution with SiO_2 [13]. The cellulose–HA nanocomposites combine the advantages of cellulose and HA, and are considered to be interesting functional materials with many potential applications in biomedical field with such striking features as high mechanical properties and excellent biocompatibility. In these nanocomposites, HA nanostructures with high specific surface area and unsaturated atoms can interact with the cellulose, leading to the enhancement of properties of the nanocomposite. The cellulose–CHA nanocomposites are considered to be interesting functional materials with many potential environmental applications with such striking features as high mechanical properties and excellent adsorption capacity. Therefore, it is greatly important to develop preparation methods for cellulose–CHA nanocomposites and to evaluate its arsenate removal efficiency.

There have been only few reports on the synthesis of cellulose–CHA nanocomposites [27–30]. For example, Yoshida et al. [26] synthesized the cellulose–CHA composites in situ through mechanochemical reaction using a conventional ball-mill. Landi et al. [27] prepared porous bodies of CHA followed by impregnation of cellulose sponges with proper slurry of the powder and optimizing the subsequent sintering. Yoshida et al. [28] reported the preparation of cellulose–CHA composites through mechanochemical reaction using poly(c-caprolactone) as plasticizer. Wang et al. [29] reported the biomimetic mineralization synthesis of calcium-deficient carbonate-contained hydroxyapatite in the three dimensional network of bacterial cellulose nanofibers by alkaline treatment.

Microwave synthesis is now used as a promising technology for the synthesis of many nanocomposites [31]. Compared with the hydrothermal method, microwave synthesis has the advantages of short reaction time, small particle size and high purity of prepared samples, and preparing highly crystalline products with narrow size distribution. Kumar et al. carried out the synthesis of hydroxyapatite (HA) nano strips by chemical precipitation method followed by microwave irradiation. The microwave assisted reactions proceed at fast rates [32]. Several researchers have attempted the synthesis of various materials via microwave assistance. Komarneni et al. demonstrated that under otherwise identical processing conditions, synthesis of crystalline hematite by a microwave approach was 36 times faster than by conventional hydrothermal methods [33]. Several studies reported the capability of controlling the particle shape and particle size with this rapid synthesis approach. Rigneau et al. further shortened the processing time to 30 min and also increased the ferric concentration to 0.05 M [34], which could increase the production rate over 100 times. The even more striking finding from their results was that the microwave synthesized Fe_2O_3 particles were nano scale. The significance of this finding is that it could not only remarkably simplify the synthesis procedure, but also get rid of the difficulties involved with the calcination of nano powders. The morphology and crystal form of the products can also be controlled by adjusting the reaction conditions [35]. Therefore, we carried out microwave assisted synthesis of cellulose–CHA nanocomposites using cellulose solution, $CaCl_2$, and NaH_2PO_4 in aqueous medium by a hydrothermal method at 180 °C for 24 h [30].

The present research investigates the feasibility of the cellulose-carbonated hydroxyapatite nanocomposites (CCHA) for As(V) removal from aqueous solution. The main objectives were (i) to understand the As(V) adsorption kinetics, (ii) to evaluate the impact of temperature, pH and coexisting anions on the As(V) removal kinetics and/or capacities; and (iii) to describe and explain some important thermodynamic parameters.

2. Experimental

2.1. Reagents and chemicals

All chemicals were of analytical grade and used as received without further purification. Stock As(V) solution (1000 mg/L) was prepared from sodium hydrogen arsenate ($Na_2HAsO_4{\cdot}7H_2O$, Merck) using distilled water. Solutions of required concentrations were obtained by serial dilution of the stock solution. All glasswares and sample bottles were soaked in 10% HNO_3 for 24 h, and finally washed with distilled water.

2.2. Sample preparation

Cellulose solution was prepared as per the method described by Jia et al. [31]. In a typical synthesis, 7 g of NaOH and 12 g of urea were added to 80 mL of distilled water under vigorous stirring to form NaOH–urea aqueous solution. Then, 3.240 g of microcrystalline cellulose (molecular weight of 34,843–38,894, degree of polymerization (DP), DP = 215–240) was added to the above solution under vigorous stirring. The above solution was cooled to 0 °C for 12 h. The obtained cellulose solution was used for the preparation of cellulose-carbonated hydroxyapatite nanocomposites (CCHA).

For the synthesis of CCHA nanocomposites, 0.110 g of $CaCl_2$ and 0.094 g of NaH_2PO_4 were added to the mixture of cellulose solution (5 mL) and distilled water (40 mL) under vigorous stirring. The above solution was heated to 90 °C for a certain time by microwave. CCHA nanocomposite synthesized was cream colored, porous, flake like structure. The product was separated from the solution by centrifugation, washed by water and ethanol and dried at 60 °C for further study.

2.3. Characterization of cellulose-carbonated hydroxyapatite

Powder XRD of the material was obtained by using PHILLIPS X'PERT X-Ray diffractometer with Cu Kα radiation (35 kV and 30 mA) at a scan rate of 1°/min and was analyzed using standard software provided with the instrument. FTIR of the sample was obtained using Perkin Elmer FTIR spectrophotometer (SPECTRUM RX–I). FTIR spectrum of the sample was obtained by KBr pellet method. The ratio of the sample to KBr was 1:50 and the pellet was prepared at a pressure of 5 Ton. Thermogravimetric analysis and differential scanning calorimetry (TGA/DSC) analysis was carried out using NETZSCH STA 409C. 30 mg of the sample was used and alumina was used as reference. TGA and DSC curve was obtained from 20 °C to 800 °C at a heating rate of 10 °C/min. Scanning electron micrograph of the sample was obtained by JEOL JSM–6480LV scanning electron microscope. The sample was coated with platinum for 30 s at a current of 50 mA and the SEM micrograph was obtained. The Ca/P molar ratio was determined by inductively connected plasma with optical emission spectroscopy (ICPOES). A Perkin Elmer Optimal 4300DV instrument was used. 0.1 g of the sample was digested in an acid sample made up of 2.5 mL of HNO_3, 1.5 mL of H_2O_2 and 0.3 mL of HCl in a 100 mL Erlenmeyer flask. The measurements of the concentration were made by triplicate on three different days.

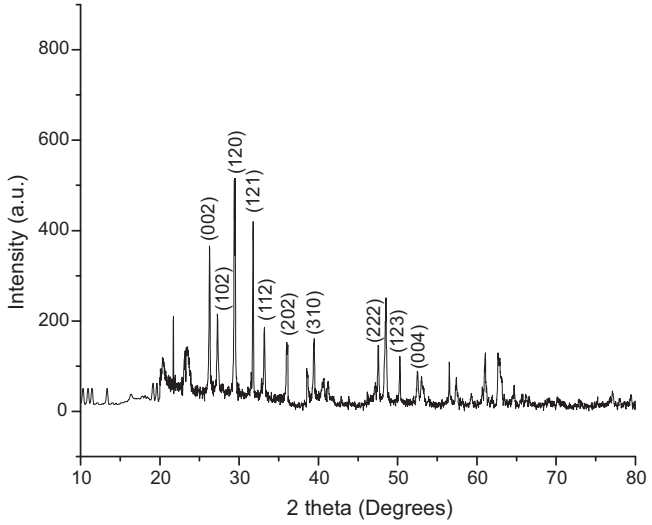

Fig. 1. XRD pattern of CCHA nanocomposite.

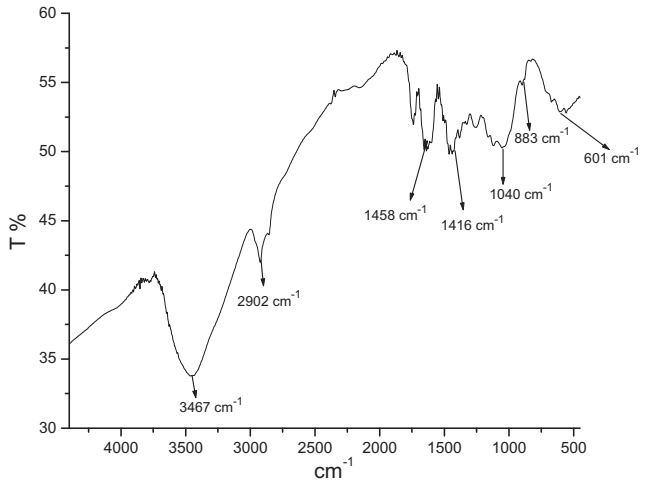

Fig. 2. FTIR spectrum of CCHA nanocomposite.

2.4. Arsenic measurement

An atomic absorption spectrometer (AAS) (Thermo Electron Corporation) equipped with an arsenic hollow cathode lamp was employed to measure arsenic concentration. An automatic intermittent hydride generation device was used to convert arsenic in water samples to arsenic hydride. The hydrides were then purged continuously by argon gas into the atomizer of an atomic absorption spectrometer for concentration measurements.

2.5. Batch experiments

The batch experiments to study the removal of As from solution were carried out by treating 50 mL of As solution in 100 mL polyethylene bottles with 0.1 g of the adsorbent. The bottles were immersed in a shaking water bath at predetermined temperature (25, 35, 45 °C). The shaker speed was controlled at 300 rpm. After a predetermined contact time, the aqueous samples in each bottle were decanted and centrifuged at 4500 rpm for 5 min, and then filtered through a 0.45 μm cellulose acetate filter. The supernatant liquid was analyzed for dissolved total As. The concentration of the As species was expressed as the element (As).

The effect of contact time (5 min – 8 h) was examined at 25 and 45 °C with initial As(V) concentrations of 10 mg/L. Adsorption isotherm studies were conducted by varying initial As(V) concentrations (1–50 mg/L) at different temperatures (i.e., 25, 35, and 45 °C). The effect of pH of the solution was investigated by adjusting the solution at different pH (2–10) using 0.05 M HCl and 0.05 M NaOH solutions with an initial As(V) concentration of 10 mg/L. To determine the effect of other competitive anions on As adsorption, batch experiments were performed using solutions of 10 mg/L As(V) containing 0.5, 1, 2, 5,10 and 20 mg/L of P (as PO_4^{3-}), N (as NO_3^-), S (as SO_4^{2-}) or Si (as SiO_3^{2-}), separately. After a 1 h contact time, the suspension was filtered through a 0.45 μm cellulose acetate filter and analyzed for total As, as described above.

3. Results and discussion

3.1. Characterization of cellulose-carbonated hydroxyapatite nanocomposite

Fig. 1 shows the X-ray powder diffraction patterns of the material. The diffraction peaks observed at around 19.9° and 21.6° in 2θ were attributed to cellulose. All the other diffraction peaks in XRD patterns can be indexed to a phase of well crystalline HA with a hexagonal structure (JCPDS 84-1998). Fourier transform infrared spectrum (Fig. 2) of the obtained material showed the typical bands at 1040 cm^{-1} (the C–O in cellulose and υ_3 PO_4^{3-}), and 601 cm^{-1} (υ_4 PO_4^{3-}), together with those at 1458 cm^{-1} (υ_{3-3} CO_3^{2-})/1416 cm^{-1} (υ_{3-4} CO_3^{2-}) and 883 cm^{-1} (υ_2 CO_3^{2-}). Apparently, CO_3^{2-} ions were in the B-site, which implied [PO_4] was partly replaced by [CO_3] [36]. The band at 2902 cm^{-1} was assigned to asymmetrically stretching vibration of C–H in pyranoid ring. Bands or shoulders at 3467 cm^{-1} is due to O–H stretching of water of crystallization. Thus, in view of the XRD and FT-IR results, the product was the cellulose–CHA nanocomposites.

The thermal stability of the cellulose–CHA nanocomposites in air was investigated using thermogravimetric analysis (TGA) and differential thermal analysis (DTA), as shown in Fig. 3. The TGA curve showed a small weight loss around 100 °C corresponding to desorption of water. The 5.5% weight loss (from TGA) around 100 °C may be attributed to the water content. The weight loss around 260 °C can be assigned to the thermal degradation and complete decomposition of cellulose in the composites [37]. The strong exothermic peaks around 350 °C were observed in the DTA curve due to decomposition of cellulose. The temperature ranges of the exothermic peaks in the DTA curve fit well with those of weight loss in the TGA curve.

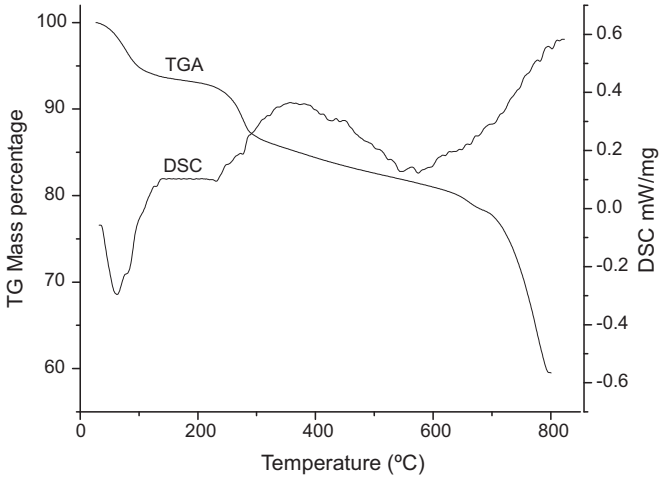

Fig. 3. Thermogravimetric analysis and differential scanning calorimetry of CCHA nanocomposite.

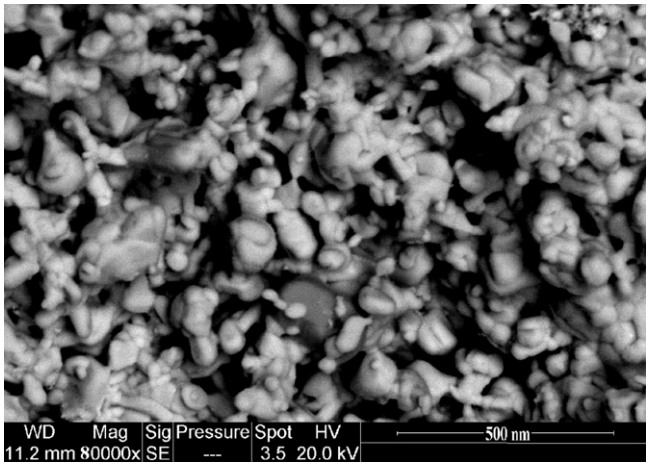

Fig. 4. SEM micrograph of CCHA nanocomposite (magnification—80,000×).

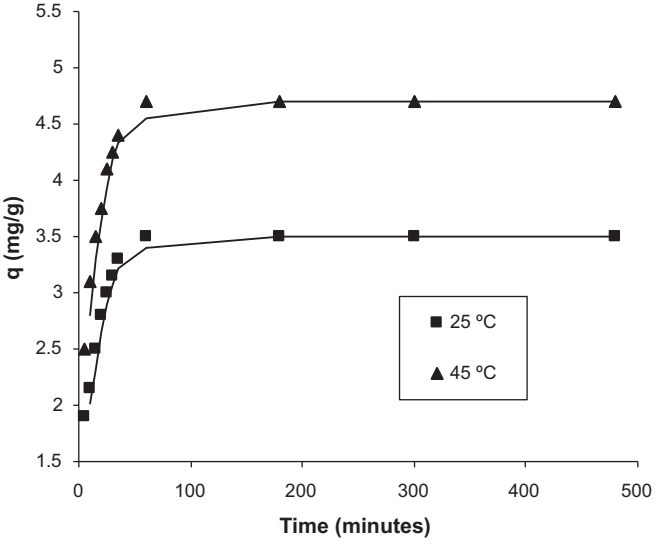

Fig. 5. Effect of contact time on As(V) adsorption on the CCHA nanocomposite (initial As(V) concentration = 10 mg/L, adsorbent dosage = 2 g/L).

The morphology of the sample was investigated with scanning electron microscopy. As shown in Fig. 4, one can see cellulose with particles and the CHA nanostructures being dispersed in the cellulose matrix. The cellulose flake with minor CHA nanostructures was also observed. Most of the CHA structures dispersed in the cellulose matrix were within the range of 20–30 nm. The cellulose and CHA have most of hydroxyl groups, which can form hydrogen bonding, making the cellulose and CHA to combine. Chemical analysis was carried out and Ca/P was found to be 2.10.

3.2. Batch experiments

3.2.1. Effect of contact time

The As(V) adsorption kinetic study was carried out with adsorbent dosage of 2 g/L and initial As concentration of 10 mg/L at 25 and 45 °C, respectively. Results are shown in Fig. 5. It demonstrates that

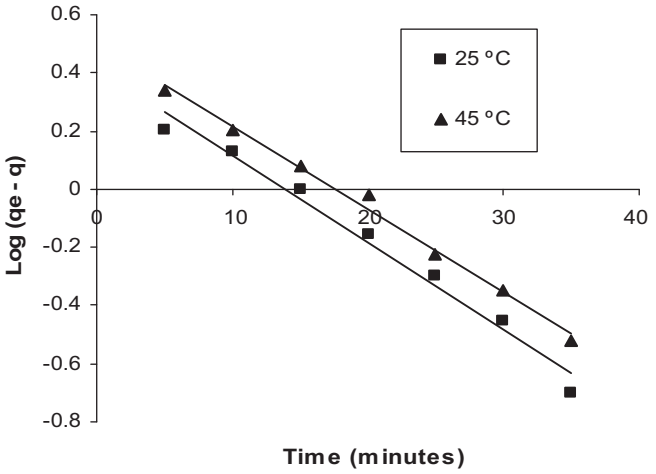

Fig. 6. Plot of Lagergren's pseudo-first-order rate for As(V) adsorption on the CCHA nanocomposite at 25 and 45 °C.

adsorbed As(V) significantly increased with an increase in contact time. The adsorption rate was rapid at the initial stage (5–30 min) and gradually slowed down afterwards. The slower adsorption was likely due to the decrease in adsorption sites on the surface of the adsorbents [38,39]. About 62% As was removed in 10 min at 45 °C, while only 43% at 25 °C. Arsenic concentration was relatively constant at contact times >60 min. The kinetic data show that As removal mainly occurred within 60 min and there was no significant change in residual As concentrations after this time up to 480 min. It means that an equilibrium of As adsorption was roughly attained within 60 min. Adsorption experiments in other batches were conducted with the contact time of 60 min.

Results also reveal that the uptake rates of As(V) increased slightly with increasing temperature (Table 1). Tyrovola et al. observed a similar trend when they used zero-valent iron for the removal of As(V) and As(III) [40]. Other investigators also reported that the As removal rate and the capacity of the adsorbents increased with increasing temperature (e.g., Mn-substituted Fe oxyhydroxide, granular ferric hydroxide, red mud [41], activated alumina [42]).

3.2.2. Adsorption kinetics

An appropriate kinetic model is often used for quantifying the changes in adsorption with time. Pseudo-first-order equation was employed to analyze the kinetic data since it allows evaluating effective adsorption capacity and the rate constant of the kinetic model without any parameters beforehand [43–47]. The pseudo-first-order Lagergren equation is shown as Eq. (1).

$$\mathrm{Log}\,(q_e - q) = \mathrm{Log}\,q_e - K_1\left(\frac{t}{2.303}\right) \quad (1)$$

where q is the amount of As(V) adsorbed at time t (mg/g), q_e is the amount of As(V) adsorbed at equilibrium (mg/g), K_1 is the equilibrium rate constant of pseudo-first-order adsorption.

The plot of Log $(q_e - q)$ versus t (contact time) is shown in Fig. 6. The straight line plots of Log $(q_e - q)$ against t had also been tested to obtain pseudo-first-order rate parameters. The K_1, q_e and correlation coefficients, R^2, values under different conditions were calculated from these plots and are given in Table 1. High cor-

Table 1
Rate constants (K_1) obtained from the graph for CCHA nanocomposite at different temperatures.

Temperature (°C)	Slope	Intercept	Rate constant in min^{-1} (K_1)	R^2
25	−0.02856	0.415207	0.065779	0.982
45	−0.02988	0.501526	0.068808	0.993

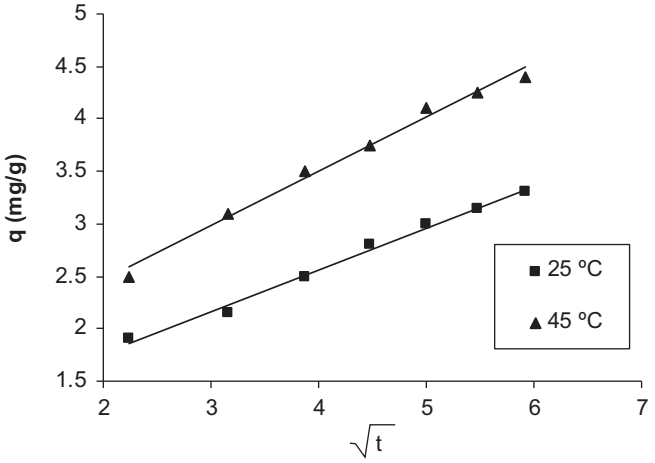

Fig. 7. Plot of Webber and Morris diffusion rate for As(V) adsorption on synthetic CCHA nanocomposite at 25 and 45 °C.

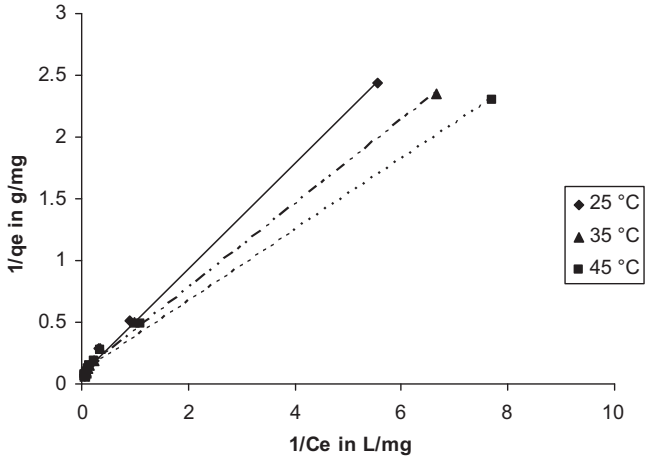

Fig. 8. Langmuir adsorption isotherm for As(V) adsorption on synthetic CCHA nanocomposite.

relation coefficients ($R^2 > 0.98$) were observed for all fits, which indicates that the adsorption reaction could be approximated with a pseudo-first-order kinetic model. It suggests that the overall rate of the As(V) adsorption process should be controlled by the chemical process in accordance with the pseudo-first-order reaction mechanism.

3.2.3. Webber and Morris model

The use of the intraparticle diffusion model has been greatly explored to analyze nature of the 'rate-controlling step', which is represented by Eq. (2) [45,47].

$$q = K_p\, t^{1/2} \tag{2}$$

where K_p is intraparticle diffusion rate constant. According to this model, if adsorption of a solute is controlled by the intraparticle diffusion process, a plot of solute adsorbed against square root of contact time should yield a straight line passing through origin. The Weber and Morris plots of As(V) adsorption on the synthetic CCHA are shown in Fig. 7. Fig. 7 indicates that the intraparticle diffusion was not the only rate-limiting step for the whole reaction. Straight lines with a great correlation coefficient ($R^2 > 0.98$) were obtained in very beginning period (within 60 mins), indicating that initial phase may be controlled by the intraparticle diffusion. The greater diffusion rate in the early stage attributed to surface adsorption and gradual adsorption. Afterwards, the intraparticle diffusion began to slow due to the low As concentration in solution [48]. The As was initially adsorbed by the exterior surface of the adsorbent. After the adsorption at the exterior surface reached the saturation, As entered the pores within the particles and was adsorbed by the interior surfaces. The diffusion resistance increased with the increase in the interior adsorption, which led to a decrease in diffusion rate [49]. With the increase in diffusion resistance and the decrease in As concentration in solution, the diffusion processes reached equilibrium. The intraparticle diffusion rate was obtained from the slope of the steep-sloped portion (initial 60 mins) (Table 2). The diffusion rate for As(V) at 45 °C is about 1.5 times faster than that at 25 °C, indicating that As was more easily diffused and transported into adsorbent pores at higher temperature.

3.2.4. Effect of initial As concentration and adsorption isotherms

Effect of initial As concentration on As adsorption were investigated at initial As(V) concentrations between 1 and 50 mg/L at 25, 35, and 45 °C. The As loadings on the adsorbents (q_e) were calculated from the equilibrium As concentrations (C_e). The adsorption loadings varied in the ranges of 0.41–15.5, 0.42–16.7 and 0.43–18.3 mg/g at 25, 35, and 45 °C, respectively. It indicates that As adsorption increased with the increase in temperature. The adsorption isotherm data (q_e versus C_e) were fitted to Langmuir and Freundlich isotherm models [Eqs. (3) and (4), respectively]. Langmuir isotherm model assumes a monolayer surface coverage limiting the adsorption due to the surface saturation, while Freundlich isotherm model is an empirical model allowing for multilayer adsorption [47].

$$\frac{1}{q_e} = \frac{1}{q_0 b C_e} + \frac{1}{q_0} \tag{3}$$

$$\log q_e = \log K_f + n \log C_e \tag{4}$$

where C_e is the equilibrium concentration in the solution (mg/L), q_e is the amount adsorbed on the adsorbent at equilibrium (mg/g), q_0 is the maximum adsorption capacity (mg/g), b is a constant related to the adsorption energy (L/mg), K_f is the Freundlich constant denoting the adsorption capacity of the adsorbent [(mg/g)(L/mg)^n], and n is the adsorption intensity parameter. Values of $0.1 < n < 1$ show favorable adsorption of As onto adsorbents. All the adsorption data obtained were fitted to both models as shown in Figs. 8 and 9. It was observed that the correlation coefficients for Langmuir isotherm model ($R^2 = 0.99$) were a little higher compared to those for Freundlich ($R^2 = 0.98$) (Table 3). Therefore, Langmuir isotherm yielded better fit to the experimental data with regard to As adsorption on CCHA at temperatures of 25, 35 and 45 °C. These facts suggest that As(V) was adsorbed in the form of monolayer coverage on the surface of the adsorbent. Langmuir isotherm model was also used to well describe As(V) adsorption on natural siderite [2], Fe oxide-coated sand [50], granular titanium dioxide adsorbent [51], synthetic goethite [52], and iron-coated sand and manganese-coated sand [53], at 25 °C.

Table 2
Intraparticle diffusion rate constants obtained from Weber–Morris equation at different temperatures.

Temperature (°C)	Slope	Intercept	Rate of pore diffusion (k_p)	R^2
25	0.39883	0.968651	0.39883	0.989
45	0.51822	1.426051	0.59822	0.992

Table 3
Langmuir and Freundlich constants for As(V) adsorption on synthetic CCHA nanocomposite at different temperatures.

Temperature (°C)	Langmuir constants			Freundlich constants		
	q_o (mg/g)	b (L/mg)	R^2	n	K_f (mg/g) (L/mg)^n	R^2
25	10.02712	0.34685	0.994	0.42104	4.05×10^{-2}	0.985
35	10.61389	0.27655	0.995	0.37916	6.02×10^{-2}	0.987
45	12.72448	0.18406	0.997	0.31555	7.75×10^{-2}	0.988

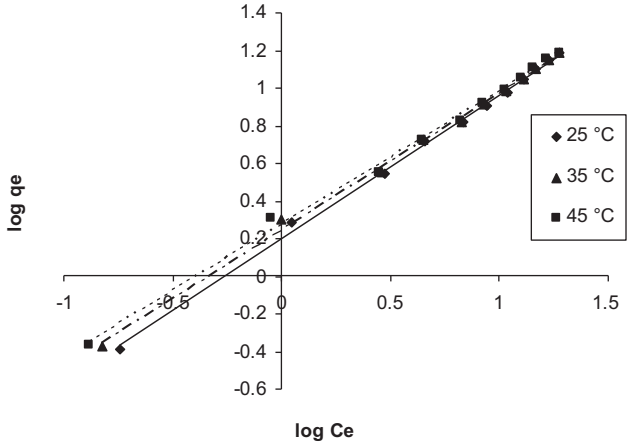

Fig. 9. Freundlich adsorption isotherm for As(V) adsorption on synthetic CCHA nanocomposite.

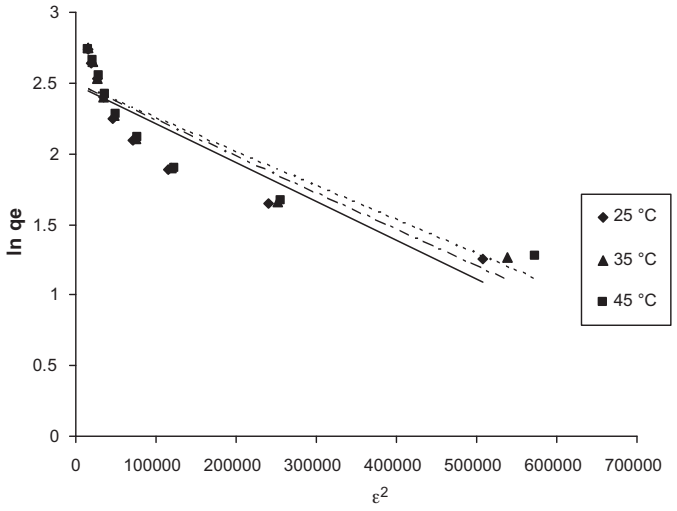

Fig. 10. DR adsorption isotherm for As(V) adsorption on synthetic CCHA nanocomposite.

The values of maximum adsorption capacity (q_o) and Langmuir constant (b) were evaluated from the intercept and slope of the Langmuir plots and given in Table 3. Results show the greatest amount of As was removed at 45 °C, followed by that at 35 and 25 °C. It demonstrates that adsorption capacity increased with an increase in reaction temperature. The arsenic adsorption capacities and the conditions at which the arsenic adsorption capacities were determined have been reported in Table 4. Arsenic adsorption capacities of various other adsorbents were compared to those reported in the literatures and were found to be more than most of them (Table 4). The values of K_f and n were obtained from the slope and intercept of the linear Freundlich plots and listed in Table 3. The K_f indicating the adsorption capacity of the adsorbent increased with an increase in reaction temperature, which is consistent with the results of Langmuir model. The calculated n lies in the range between 0.3 and 0.5, denoting favorable adsorption of As(V) onto the synthetic CCHA.

It is known that the Langmuir and Freundlich adsorption isotherm constant do not give any idea about the adsorption mechanism. In order to understand the adsorption type, equilibrium data were tested with Dubinin–Radushkevich isotherm. The linearized D.R. equation can be written as [47];

$$\ln q_e = \ln q_m - K\varepsilon^2 \quad (5)$$

where ε is polanyi potential, and is equal to $RT\ln(1+1/C_e)$, q_e is the amount of arsenate adsorbed per unit mass of adsorbent, q_m is the theoretical adsorption capacity, C_e is the equilibrium concentration of arsenate, K is the constant related to adsorption energy, R is universal gas constant and T is the temperature in Kelvin. Fig. 10 shows the plot of $\ln q_e$ against ε^2, which was almost linear with correlation coefficients, $R^2 > 0.97$. D.R. isotherm constants K and q_m were calculated from the slope and intercept of the plot, respectively. The values of K were found to be 0.00278, 0.00245 and 0.00243 mol^2 kJ^{-2} and those of q_m were 7.3952, 7.4563, 7.5575 mg/g at 25, 35 and 45 °C respectively. The mean free energy of adsorption (E) was calculated from the constant K using Eq. (6) [46,47].

$$E = (2K)^{-1/2} \quad (6)$$

E is defined as the free energy change when 1 mol of ion is transferred to the surface of the solid from infinity in solution. The values of E were found to be 13.411, 14.285 and 14.244 kJ mol^{-1} at 25, 35 and 45 °C respectively. The value of E is very useful in predicting the type of adsorption. If the value of E is <8 kJ mol^{-1}, then the adsorption is physical in nature and if it is in between 8 and 16 kJ mol^{-1},

Table 4
Adsorption capacities of different adsorbents reported in the literatures.

Adsorbents reported in the literatures and CCHA nanocomposite	Adsorption capacity of As(V)/As (III) adsorption (in mg/g)		pH	Concentration	References
CCHA nanocomposite	12.72	As (V)	7.0	1–50 mg/L	Present research
Activated alumina	0.18	As (III)	7.6	0.5–1.5 mg/L	[42]
Waste Fe(III)/Cr(III) hydroxides	11.02	As (V)	4.0	20–100 mg/L	[54]
Activated bauxsol	7.64	As (V)	4.5	7.03–220.9 μmol/L	[41]
Bauxsol	1.08	As (V)	4.5	0.80–32.0 μmol/L	[55]
Mixed rare earth oxide	2.95	As (V)	6.5	50 mg/L	[56]
Titanium dioxide Amberlite XAD-7	4.72	As (V)	4.0	0–5 mmol/L	[57]
Goethite	4.00	As (V)	9.0	0–60 mg/L	[58]
Calcined LDH	5.61	As (V)	4.2	20–200 mg/L	[59]

Table 5
Thermodynamic parameters for As(V) adsorption on synthetic CCHA nanocomposite at different temperatures.

Temperature (°C)	ΔG° (kJ/mol)	ΔH° (kJ/mol)	ΔS° (J/(mol K))
25	−2.626		92.387
35	−3.295	24.905	91.559
45	−4.480		92.405

then the adsorption is due to exchange of ions [46,47]. The values found in the present study were in between 8 and 16 kJ mol^{-1}. So, the adsorption can be best explained as ion exchange. The probable arsenate adsorption is due to the exchange of phosphate ions present in CCHA nanocomposite by the arsenate ions present in the synthetic arsenate solution. In addition to ion-exchange there is a possibility of physical adsorption on the surface of CCHA nanocomposite.

3.2.5. Thermodynamic study

To evaluate the thermodynamic feasibility and to confirm the nature of the adsorption process, three basic thermodynamic parameters, standard free energy (ΔG°), standard enthalpy (ΔH°) and standard entropy (ΔS°) were calculated using the following equations [Eqs. (7)–(9)].

$$\Delta G^\circ = -RT \ln\left(\frac{1}{b}\right) \quad (7)$$

$$\ln b = \ln b_O - \frac{\Delta H^\circ}{RT} \quad (8)$$

$$\Delta G^\circ = \Delta H^\circ - T\Delta S^\circ \quad (9)$$

where b is Langmuir constant which is related to the energy of adsorption, b_0 is a constant, R is the universal gas constant (8.314 J/(mol K)), and T is the temperature in Kelvin (K). Calculated values of the thermodynamic parameters ΔG°, ΔH° and ΔS° are given Table 5. The negative ΔG° values indicate the adsorption process was spontaneous. The value of ΔH° for As(V) adsorption is 24.905 kJ/mol, suggesting that interaction between As(V) and the synthetic CCHA was endothermic in nature. Hence, it can be concluded that the nature of As(V) adsorption was chemical (ion-exchange), which is consistent with the results of kinetic study. The decrease in ΔG° with the rise in temperature shows an increase in feasibility of adsorption at higher temperatures. The positive ΔS° values indicate some structural changes in adsorbate and adsorbent during adsorption reaction.

3.2.6. Effect of solution pH

The solution pH is an important parameter, which influences most of the solid/liquid adsorption processes. The adsorption of As(V) on the synthetic CCHA was examined at different pH ranging from 2 to 10 with an initial As(V) concentration of 10 mg/L and a contact time of 1 h. Results are presented in Fig. 11. The pH of water may affect the degree of ionization of the sorbate and the surface charge of the sorbent. The percentage removal of arsenate by CCHA increased from 65% to 70%, for increase in pH from 2 to 4 and then the percentage removal decreased from 70% to 45% with increase in pH from 8 to 10. It is evident from the above data that there was increase in percentage removal for increase in pH from 2 to 4. It may be due to the fact that CCHA is not stable under acidic condition and hence exhibited poor removal efficiency. But for further increase in pH beyond 8, there was decrease in percentage removal.

The electrophoretic studies are important in view of determination of behavior of adsorbent materials in different electrolytic medium. The point of zero charge (pH_{pzc}) was determined using electrophoretic mobility in a solution of ionic strength 0.01 M NaCl and 0.001 M NaCl (Fig. 12). The point at which the zeta potential was found to be zero is termed as point of zero charge. From the electrophoretic study shown graphically as a plot of pH versus the zeta potential (in mV), the point of zero charge values of CCHA nanocomposite was found to be 8 at both 0.01 M and 0.001 M NaCl solution. Above this pH (pH_{pzc}), the surface is negative (repels anions) while below this point the surface charge is positive. This may be the probable reason for the decrease in adsorption capacity of the negative arsenate anion at pH > 8.

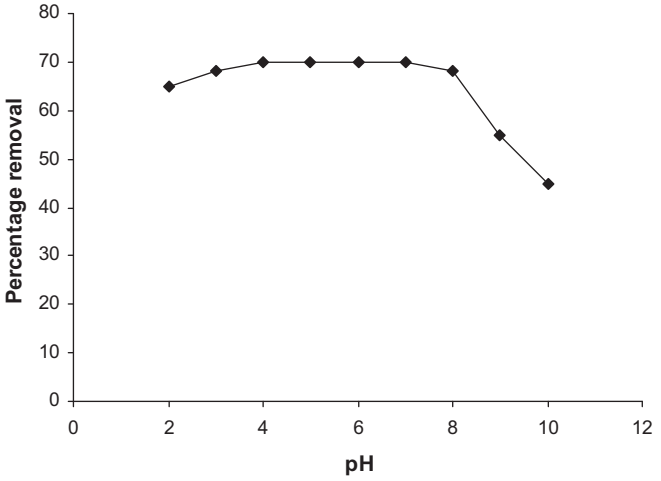

Fig. 11. Effect of solution pH on As(V) adsorption onto synthetic CCHA nanocomposite (initial As(V) concentration = 10 mg/L, temperature = 25 °C, contact time = 1 h, adsorbent dosage = 2 g/L).

3.2.7. Effect of competing anions on As removal

Arsenic(V) adsorption in the presence of competing anions (including NO_3^-, SO_4^{2-}, PO_4^{3-}, or SiO_3^{2-}) was investigated with 0.5, 1, 2, 5,10 and 20 mg/L of P (as PO_4^{3-}), N (as NO_3^-), S (as SO_4^{2-}), or Si (as SiO_3^{2-}) with an initial As(V) concentration of 10 mg/L at 25 °C. Results are shown in Fig. 13. The adverse effect of the anion on As(V) removal decreased in the following order: $SiO_3^{2-} > PO_4^{3-} > NO_3^- > SO_4^{2-}$. The removal of As(V) decreased significantly as PO_4^{3-} and SiO_3^{2-} concentrations increased in the separate solutions. Sulphate (SO_4^{2-}) does not significantly affect the As(V) adsorption (Fig. 13). The SO_4^{2-} had no obvious effect on adsorption of As(V) because it did not compete with arsen-

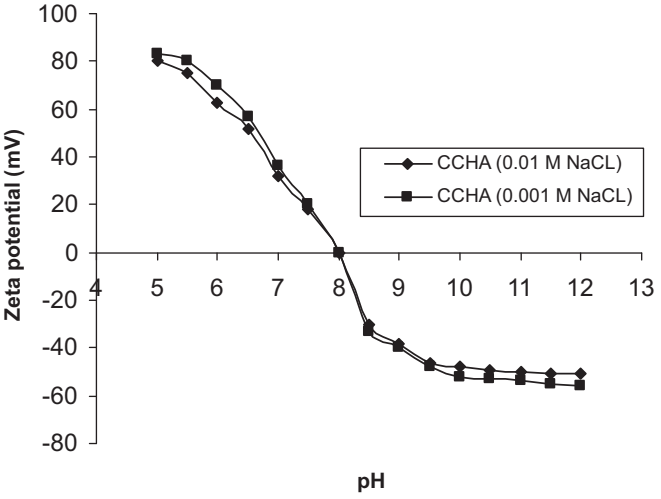

Fig. 12. Zeta of CCHA nanocomposite as a function of pH using 0.01 M NaCl and 0.001 M NaCl as supporting electrolyte.

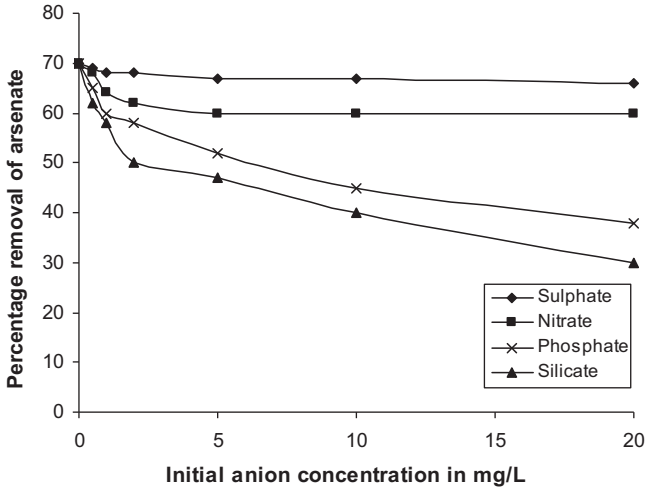

Fig. 13. Effect of presence of anions on As(V) adsorption (initial As(V) concentration = 10 mg/L, temperature = 25 °C, contact time = 1 h, adsorbent dosage = 2 g/L).

ate. With the presence of 0.5 mg/L N (as NO_3^-), removal efficiency reduced from 70% to 61% in comparison with the absence of NO_3^-. Above 2 mg/L N (as NO_3^-), the effect leveled off. As can be seen from Fig. 13, an increase in Si from 0.5 to 10 mg/L resulted in a decrease in removal efficiency from 70% to 40%, which amounts to a 30% decrease in As(V) adsorption. Above 10 mg/L Si, the adverse effect was even stronger. At 20 mg/L Si, the removal efficiency reduced to 30%. The probable reason for decrease in percentage removal with increase in the concentration of competing anions can be explained, by considering ionic radii of the competing anions. The ionic radii of the anions follow the order of arsenate > silicate > phosphate > sulphate > nitrate. It has been observed that the anions with large ionic radii decreased the percentage arsenate removal to a large extent. So, silicates and phosphates have large effect on arsenate removal whereas nitrates and sulphates have less effect on the arsenate removal. Meng et al. also found that As removal by Fe hydroxides was reduced from greater than 99% to approximately 85% when silicate concentration was increased from 0.6 mM to approximately 0.7 mM [60]. In contrast, Zhang et al. observed a 30% decrease in As(V) adsorption when Si (as silicate) concentration increased from 1.4 to 5 mg/L [22]. Below 2 mg/L P as PO_4^{3-}, the change of As removal efficiency with PO_4^{3-} concentration is almost same as SiO_3^{2-}. With an increase in P concentration from 0.5 to 20 mg/L, the As(V) removal efficiency steadily reduced from 70% to 38%. The evident decrease in As(V) removal in the presence of PO_4^{3-} and SiO_3^{2-} was believed to result from the competitive adsorption between As(V) and those anions. Guo et al. [2] also found that the presence of phosphate (10 mg/L in terms of P) reduced the uptake of As(V) by natural siderite from 54% to 28%. In Inner Mongolia, most high As groundwater had P concentrations ranging from <0.1 mg/L to 3.54 mg/L and Si concentrations from 3.5 mg/L to 16.9 mg/L [61,62]. It was speculated that the component adversely affecting As removal efficiency should be SiO_3^{2-} rather than PO_4^{3-} in case that the adsorbent is applied to remove As from high As groundwater in Inner Mongolia. There are several other studies which report the arsenic contamination in drinking water and the effect of competing ions on arsenic removal [63–65]. Effect of background electrolyte (NaCl) concentration was investigated with 0.001–0.1 mol/L NaCl as background electrolyte with an initial As(V) concentration of 10 mg/L at 25 °C. It was found that As(V) removal was not affected by the concentration of background electrolyte.

4. Conclusion

Microwave assisted synthesis of CCHA nanocomposite was carried out using cellulose solution, $CaCl_2$, and NaH_2PO_4. Synthesis was ascertained by adopting various characterizing methods like SEM, XRD, FTIR and TGA–DSC. Arsenate removal efficiency was evaluated by studying the effect of various parameters on the effectiveness of treating synthetic arsenate solution. As(V) adsorption on the synthetic CCHA was complete within 60 min. The adsorption rate was fast at the initial stage, followed by a slower rate, which well fitted the Lagergren first order kinetic model. Equilibrium was established within 60 min. Temperature played an important role in the As(V) adsorption capacity. At higher temperature, As(V) exhibited greater removal degrees. The adsorption closely followed Langmuir isotherm at different temperatures. pH of a solution affects both the surface charge of the material and the speciation of As(V). The point of zero charge values of CCHA nanocomposite was found to be 8 at both 0.01 M and 0.001 M NaCl solution. This may be the probable reason for the decrease in adsorption capacity of arsenate anion at pH > 8. Thermodynamic study shows that As(V) adsorption onto the synthetic CCHA was an endothermic process, indicating As(V) adsorption capacity increased with an increase in reaction temperature. The adsorption was spontaneous and favorable at the temperature investigated. As(V) removal varied between 65 and 71% between pH 4 and 8. The presence of SO_4^{2-} and NO_3^- had no significant effect on the uptake of As(V) by CCHA, while PO_4^{3-} and SiO_3^{2-} impeded As(V) adsorption.

Acknowledgements

The authors are thankful to Prof. P.C. Panda (Director), Prof. K.M. Purohit, and staff members of department of chemistry, National Institute of Technology, Rourkela, for providing necessary facilities and necessary help in carrying out the research work. The authors are also thankful to Prof. U.C. Patra (Director), Purushottam Institute of Engineering & Technology, Rourkela, and other staffs for their necessary help and cooperation.

References

[1] P.L. Smedley, D.G. Kinniburgh, A review of the source, behaviour and distribution of arsenic in natural waters, Appl. Geochem. 17 (2002) 517–568.
[2] H.M. Guo, D. Stuben, Z. Berner, Removal of arsenic from aqueous solution by natural siderite and hematite, Appl. Geochem. 22 (2007) 1039–1051.
[3] A.K. Singh, Approaches for removal of arsenic from groundwater of northeastern India, Curr. Sci. 92 (2007) 1506–1515.
[4] J.C. Ng, J.P. Wang, A. Shraim, A global health problem caused by arsenic from natural sources, Chemosphere 52 (2003) 1353–1359.
[5] M. Vahter, L. Li, B. Nermell, A. Rahman, S. Arifeen, M. Rahman, L.A. Persson, E.C. Ekstrom, Arsenic, a global public health problem, Toxicol. Lett. 164 (2006) S45–S46.
[6] A.H. Smith, E.O. Lingas, M. Rahman, Contamination of drinking-water by arsenic in Bangladesh: a public health emergency, Bull. World Health Org. 78 (2000) 1093–1103.
[7] Y. Xia, J. Liu, An overview on chronic arsenism via drinking water in PR China, Toxicology 198 (2004) 25–29.
[8] K.C. Saha, Review of arsenicosis in West Bengal, India—a clinical perspective. Critical review, Environ. Sci. Technol. 30 (2003) 127–163.
[9] Technologies and Costs for Removal of Arsenic from Drinking Water, U.S. Environmental Protection Agency, Washington, DC, 2000.
[10] C. Christen, New Jersey proposes toughest arsenic standard worldwide, Environ. Sci. Technol. 38 (2004) 105A.
[11] S.R. Wickramasinghe, B. Han, J. Zimbron, Z. Shen, M.N. Karim, Arsenic removal by coagulation and filtration: comparison of groundwaters from the United States and Bangladesh, Desalination 169 (2004) 224–231.
[12] L. Wang, A.S.C. Chen, T.J. Sorg, K.A. Fields, Field evaluation of As removal by IX and AA, J. AWWA 94 (2002) 161–173.
[13] A. Nakahira, T. Okajima, T. Honma, S. Yoshioka, I. Tanaka, Arsenic removal by hydroxyapatite-based ceramics, Chem. Lett. 35 (2006) 856–857.
[14] I.A. Katsoyiannis, A.I. Zouboulis, Removal of arsenic from contaminated water sources by sorption onto iron-oxidecoated polymeric materials, Water Res. 36 (2002) 5145–5155.
[15] E. Korngold, N. Belayev, L. Aronov, Removal of arsenic from drinking water by anion exchange, Desalination 141 (2001) 81–84.

[16] Y. Sato, M. Kang, T. Kamei, Y. Magara, Performance of nanofiltration for arsenic removal, Water Res. 36 (2002) 3371–3377.
[17] P.R. Kumar, S. Chaudhari, K.C. Khilar, S.P. Mahajan, Removal of arsenic from water by electrocoagulation, Chemosphere 55 (2004) 1245–1252.
[18] M. Arienzo, P. Adamo, J. Chiaenzelli, M.R. Bianco, A. de Martino, Retention of arsenic on hydrous ferric oxides generated by electrochemical peroxidation, Chemosphere 48 (2002) 1009–1018.
[19] I.A. Katsoyiannis, A.I. Zouboulis, Application of biological processes for the removal of arsenic from groundwaters, Water Res. 38 (2004) 17–26.
[20] O.S. Thirunavukkarasu, T. Viraraghavan, K.S. Subramanian, Arsenic removal from drinking water using iron oxidecoated sand, Water Air Soil Pollut. 142 (2003) 95–111.
[21] A. Chiba, H. Okada, T. Tada, H. Kudo, H. Nakazawa, K. Mitsuhashi, T. Ohara, H. Wada, Removal of arsenic from geothermal water by high gradient magnetic separation, IEEE Trans. Appl. Supercond. 12 (2002) 952–954.
[22] W. Zhang, P. Singh, P. Paling, F. Delides, Arsenic removal from contaminated water by natural iron ores, Miner. Eng. 17 (2004) 517–524.
[23] O.S. Thirunavukkarasu, T. Viraraghavan, K.S. Subramanian, O. Chaalal, M.R. Islam, Arsenic removal in drinking water—impacts and novel removal technologies, Energy Source 27 (2005) 209–219.
[24] M. Bissen, F.H. Frimmel, Arsenic—a review. Part II: oxidation of arsenic and its removal in water treatment, Acta Hydrochim. Hydrobiol. 31 (2003) 97–107.
[25] L. Hong, Y.L. Wang, S.R. Jia, Y. Huang, C. Gao, Y.Z. Wan, Hydroxyapatite/bacterial cellulose composites synthesized via a biomimetic route, Mater. Lett. 60 (2006) 1710–1713.
[26] A. Yoshida, T. Miyazaki, M. Ashizuka, E. Ishida, Bioactivity and mechanical properties of cellulose/carbonate hydroxyapatite composites prepared in situ through mechanochemical reaction, J. Biomater. Appl. 21 (2006) 179–194.
[27] E. Landi, G. Celotti, G. Logroscino, A. Tampieri, Carbonated hydroxyapatite as bone substitute, J. Eur. Ceram. Soc. 23 (2003) 2931–2937.
[28] A. Yoshida, T. Miyazaki, E. Ishida, M. Ashizuka, Preparation of cellulose-carbonate apatite composites through mechanochemical reaction, Key Eng. Mater. 284–286 (2005) 855–858.
[29] S. Shi, S. Chen, X. Zhang, W. Shen, X. Li, W. Hu, H. Wang, Biomimetic mineralization synthesis of calcium-deficient carbonate-containing hydroxyapatite in a three-dimensional network of bacterial cellulose, J. Chem. Technol. Biotechnol. 84 (2009) 285–290.
[30] J.F. Zhu, Y.J. Zhu, M.G. Ma, L.X. Yang, L. Gao, Simultaneous and rapid microwave synthesis of polyacrylamide-metal sulfide (Ag_2S, Cu_2S, HgS) nanocomposites, J. Phys. Chem. C 111 (2007) 3920–3926.
[31] N. Jia, S.M. Li, M.G. Ma, R.C. Sun, J.F. Zhu, Hydrothermal synthesis and characterization of cellulose-carbonated hydroxyapatite nanocomposites in NaOH–urea aqueous solution, Sci. Adv. Mater. 2 (2010) 210–214.
[32] A.R. Kumar, S. Kalainathan, A.M. Saral, Microwave assisted synthesis of hydroxyapatite nano strips, Cryst. Res. Technol. 45 (2010) 776–778.
[33] S. Komarneni, V.C. Menon, Q.H. Li, Synthesis of ceramic powders by novel microwave-hydrothermal processing, Ceram. Trans. 62 (1996) 1042–1122.
[34] P. Rigneau, K. Bellon, I. Zahreddine, D. Stuerga, Microwave flash-synthesis of iron oxide nanoparticles, Eur. Phys. J. Appl. Phys. 7 (1999) 41–43.
[35] J.F. Zhu, Y.J. Zhu, Microwave-assisted one-step synthesis of polyacrylamide-metal (M = Ag, Pt, Cu) nanocomposites in ethylene glycol, J. Phys. Chem. B 110 (2006) 8593–8597.
[36] Q. He, Z. Huang, Y. Liu, W. Chen, T. Xu, Template-directed one-step synthesis of flowerlike porous carbonated hydroxyapatite spheres, Mater. Lett. 61 (2007) 141–143.
[37] H. Zheng, J. Zhou, Y. Du, L. Zhang, Cellulose/chitin films blended in NaOH/urea aqueous solution, J. Appl. Polym. Sci. 86 (2002) 1679–1683.
[38] C. Su, R.W. Puls, Arsenate and arsenite removal by zero-valent iron: kinetics, redox transformation, and implications for in situ groundwater remediation, Environ. Sci. Technol. 35 (2001) 1487–1492.
[39] S. Goldberg, Competitive adsorption of arsenate and arsenite on oxides and clay minerals, Soil Sci. Soc. Am. J. 66 (2002) 413–421.
[40] K. Tyrovola, N.P. Nikolaidis, N. Veranis, N. Kallithrakas-Kontos, P.E. Koulouridakis, Arsenic removal from geothermal waters with zero-valent iron—effect of temperature, phosphate and nitrate, Water Res. 40 (2006) 2375–2386.
[41] H. Genc-Fuhrman, J.C. Tjell, D. Mcconchie, Adsorption of arsenic from water using activated neutralized red mud, Environ. Sci. Technol. 38 (2004) 2428–2434.
[42] T.S. Singh, K.K. Pant, Equilibrium, kinetics and thermodynamic studies for adsorption of As(III) on activated alumina, Sep. Purif. Technol. 36 (2004) 139–147.
[43] M. Islam, R.K. Patel, Evaluation of removal efficiency of fluoride from aqueous solution using quick lime, J. Hazard. Mater. 143 (2007) 303–310.
[44] M. Islam, R.K. Patel, Polyacrylamide thorium (IV) phosphate as an important lead selective fibrous ion exchanger: synthesis, characterization and removal study, J. Hazard. Mater. 156 (2008) 509–520.
[45] M. Islam, R.K. Patel, Nitrate sorption by thermally activated Mg/Al chloride hydrotalcite like compound, J. Hazard. Mater. 169 (2009) 524–531.
[46] M. Islam, R.K. Patel, Removal of lead (II) from aqueous environment by a new fibrous ion exchanger: polycinnamamide thorium (IV) phosphate, J. Hazard. Mater. 172 (2009) 707–715.
[47] M. Islam, R.K. Patel, Synthesis & physicochemical characterization of Zn/Al chloride layered double hydroxide and evaluation of its nitrate removal efficiency, Desalination 256 (2010) 120–128.
[48] M. Badruzzaman, P. Westerhoff, D.R.U. Knappe, Intraparticle diffusion and adsorption of arsenate onto granular ferric hydroxide (GFH), Water Res. 38 (2004) 4002–4012.
[49] Y. Kim, C. Kim, I. Choi, S. Rengaraj, J. Yi, Arsenic removal using mesoporous alumina prepared via a templating method, Environ. Sci. Technol. 38 (2004) 924–931.
[50] O.S. Thirunavukkarasu, T. Viraraghavan, K.S. Subramanian, Arsenic removal from drinking water using Fe oxide-coated sand, Water Air Soil Pollut. 142 (2003) 95–111.
[51] S. Bang, M. Patel, L. Lippincott, X. Meng, Removal of arsenic from groundwater by granular titanium dioxide adsorbent, Chemosphere 60 (2005) 389–397.
[52] P. Lakshmipathiraj, B.R.V. Narasimhan, S. Prabhakar, G. Bhaskar Raju, Adsorption of arsenate on synthetic goethite from aqueous solutions, J. Hazard. Mater. B136 (2006) 281–287.
[53] Y.Y. Chang, K.H. Song, J.K. Yang, Removal of As(III) in a column reactor packed with iron-coated sand and manganese-coated sand, J. Hazard. Mater. 150 (2008) 565–572.
[54] C. Namasivayam, S. Senthilkumar, Removal of arsenic (V) from aqueous solution using industrial solid waste: adsorption rates and equilibrium studies, Ind. Eng. Chem. Res. 37 (1998) 4816–4822.
[55] H. Genc-Fuhrman, J.C. Tjell, D. McConchie, Increasing the arsenate adsorption capacity of neutralized red mud (Bauxsol), J. Colloid Interface Sci. 271 (2004) 313–320.
[56] A.M. Raichur, V. Penvekar, Removal of As(V) by adsorption onto mixed rare earth oxides, Sep. Sci. Technol. 37 (2002) 1095–1108.
[57] B. Tatineni, M. Hideyuki, Adsorption characteristics of As(III) and As(V) with titanium dioxide loaded Amberlite XAD-7 resin, Anal. Sci. 18 (2002) 1345–1349.
[58] V. Lenoble, O. Bouras, V. Deluchat, B. Serpaud, J.-C. Bollinger, Arsenic adsorption onto pillared clays and iron oxides, J. Colloid Interface Sci. 255 (2002) 52–58.
[59] L. Yang, Z. Shahrivari, P.K.T. Liu, M. Sahimi, T.T. Tsotsis, Removal of trace levels of arsenic and selenium from aqueous solutions by calcined and uncalcined layered double hydroxides (LDH), Ind. Eng. Chem. Res. 44 (2005) 6804–6815.
[60] X.G. Meng, G.P. Korfiatis, S. Bang, K.W. Bang, Combined effects of anions on arsenic removal by iron hydroxides, Toxicol. Lett. 133 (2002) 103–111.
[61] H.M. Guo, S.Z. Yang, X.H. Tang, Y. Li, Z.L. Shen, Groundwater geochemistry and its implications for arsenic mobilization in shallow aquifers of the Hetao Basin, Inner Mongolia, Sci. Total Environ. 393 (2008) 131–144.
[62] P.L. Smedley, M. Zhang, G. Zhang, Z. Luo, Mobilisation of arsenic and other trace elements in fluviolacustrine aquifers of the Huhhot Basin, Inner Mongolia, Appl. Geochem. 18 (2003) 1453–1477.
[63] A.M. Cooper, K.D. Hristovski, T. Möller, P. Westerhoff, P. Sylvester, The effect of carbon type on arsenic and trichloroethylene removal capabilities of iron (hydr)oxide nanoparticle-impregnated granulated activated carbons, J. Hazard. Mater. 183 (2010) 381–388.
[64] D.A. Lytle, A.S. Chen, T.J. Sorg, S. Phillips, K. French, Microbial As(III) oxidation in water treatment plant filters, J. Am. Water Works Assoc. 99 (2007) 72–86.
[65] B. An, Z. Fu, Z. Xiong, D. Zhao, A.K. Sengupta, Synthesis and characterization of a new class of polymeric ligand exchangers for selective removal of arsenate from drinking water, React. Funct. Polym. 70 (2010) 497–507.